International Journal of Computer Engineering & Technology (IJCET)
Volume 8, Issue 4, July-August 2017, pp. 138–145, Article ID: IJCET_08_04_015
Available online at
http://www.iaeme.com/ijcet/issues.asp?JType=IJCET&VType=8&IType=4
Journal Impact Factor (2016): 9.3590(Calculated by GISI) www.jifactor.com
ISSN Print: 0976-6367 and ISSN Online: 0976–6375

ROBUST SEGMENTATION OF DEFORM OBJECTS USING MORPHOLOGICAL SCALE SPACE

Haythem El-Messiry
School of Engineering and Information Technology,
Al Dar University College, Dubai

ABSTRACT

The paper presents a method towards a robust segmentation that can be used in sequential images. The proposed method combines low-high level methods, which asserts prior information about local structure around control points along the deformable boundary. The method has ability to preserve multi resolution, and the localization of sharp-edges by taking the advantage of using the morphological scale-space by decomposing the image into a number of scales of different structure size. The method was tested on sequential of medical images 23 frames per heart cycle and compared to two other approaches. The estimated boundary converges correctly to the main contour with maximum distance error 5 pixels over all control points.

Key word: Segmentation, deform, morphological scale space, robust.

Cite this Article: Haythem El-Messiry, Robust Segmentation of Deform Objects Using Morphological Scale Space. *International Journal of Computer Engineering & Technology*, 8(4), 2017, pp. 138–145.
http://www.iaeme.com/ijcet/issues.asp?JType=IJCET&VType=8&IType=4

1. INTRODUCTION

A fundamental problem in image processing and computer vision is the segmentation of the deforming objects with complex motions especially medical organs. A challenging problem is to segment regions with boundary insufficiencies, i.e., missing edges and/or lack of texture contrast between regions of interest (ROIs) and background. The major problems related to the boundary's detection are the typical shortcomings of' discrete data, such as sampling artifacts and noise, which may cause the shape boundaries to be indistinct and disconnected. In addition the artifacts are around the edges. Thus, segmentation appears error prone and often incomplete [3]. There exit a number of' different approaches that employ different models for segmentation. For example approaches are based on deformable models, specially the active contour models and their extensions [5] but most of the applied techniques fails in over passing the surrounded appearance structures. A method is presented that combines a low level approach, which gives a good initialization position since the approach determines the inner cavity and over passes the artifacts

surrounding the boundary. With a high-level approach in one framework, through building a statistical model that describes the variability in border instantiation in terms of prior distribution on deformations of a template.

2. METHOD

Low-level, pixel-based method that uses a multi-scale analysis technique based on mathematical morphology; features are derived after mapping them into a nonlinear scale-space. Low-level method operating on pixels has the potential to reduce errors made in model-based approaches, due to inaccurate prior assumptions about the salient image features. The used multi-scale analysis differs from most low-level methods that use multi-scale analysis, in that it utilizes the derived features using defined descriptor scales which allow independent structure analysis. Then building the knowledge based model [1], we can direct the estimated contour to the best fit to the edge. The method has three main stages:

- Low-level stage: The processing starts with a bottom-up multi-scale analysis, based mainly on morphological scale-space by decomposing the image into a number of scales of different size of structuring element. As a result of the decomposition, the gray level appearance structures adjacent to the border are located, and finally an estimated boundary is obtained irrespective to the details of such structures.
- High-level stage: Prior information about local structure around defined points along the shape boundary is asserted.
- Combined low-high level stage: Refinement the estimated contour from low level stage, using the high-level stage to the accurate segmentation for the border.

3. LOW LEVEL VISUAL STAGE

3.1. Morphological Scale-Space

Mathematical morphology is a nonlinear analysis of signals, using structuring elements. Two dual operations, erosion and dilation, are the most basic morphological operators. Erosion is shrinking operation while dilation is an expanding one. By combining dilation and erosion two new operations opening and closing can be defined. The Morphological band-pass filter is defined according to [1, 4], by the following formula:

$$
\begin{aligned}
&n \geq 0: \\
&H_{n+1} = f \\
&B_n = (H_{n+1} \bullet d_n) \\
&H_n = H_{n+1} - B_n
\end{aligned}
\qquad (1)
$$

where is either the opening or the closing operator, *f* the given image.

The resulting B_n represent a morphological decomposition of the image into bands of different structure sizes with light and dark blobs (limited with structure size d_n). H_n are intermediate high-pass filtered images. Equation (1) shows a recursive algorithm that alternately high- and low pass filters the image starting with high-pass filtering at the coarsest scales.

3.2. Closing and Opening Descriptor Scales

The Descriptor scale is defined as the scale that maximizes the response of the band-pass morphological filter at each point in the image. This scale gives constant values in a region of constant width, using the definition given by [2], the difference that we defined a descriptor scale for each morphological scale-space obtained from the opening-closing operators separately. According to the equation:

$$S_D = \arg_{S_k}\left(\max_{S_k=S_1,\ldots\ldots,S_n}\left|\frac{B_{S_k}}{S_{k+1}-S_k}\right|\right)_D \qquad (2)$$

Consequently, the best scale that represents the inner region of deformable model is selected from the complete scale space. In addition any artifact around the deformable contour is determined by different scales among the scale space which leads to an estimated contour passing any artifact.

4. HIGH LEVEL VISUAL STAGE

Most of the high-level approaches based on the Active Shape Model (ASM) [6] and Active Appearance Model (AAM) [7] depend on building a shape model and an appearance model to describe an object. Instead the predicted shape given by the morphological scale-space approach (low-level process), is used as an initialization without the need to build a statistical model of shape variation. In addition an appearance model around selected points is built along the shape (high-level process); in order to guide the estimated contour to the accurate fit to the boundary.

4.1. Building the Knowledge-Based Model

Labeling the Training Set

For generating a training set in the new proposed technique, each boundary of the training image is represented by a set of labeled points. The number of points should be large enough to show the overall boundary.

Control Points Selection

From the generated set of labeled points a set of control points is selected, which are separated by equal orientation and located along a certain path using the following:

1. Calculate the average center of mass for all labeled boundaries of the training images (in order to align the labeled points of the training boundaries into a common coordinate frame).

2. For each training image do:

(a) Take the average center of mass of the closed contours calculated from step 1 as the point of origin.

(b) Perform a radial decomposition to the region into wedges with 30_ opening with 15_ overlap, along the labeled boundary.

(c) Select the intersection point of the wedge regularity lies on the labeled boundary as a control point. The vector describing the n control points of the boundary in the training set is

$$V = (x_1, y_1, x_2, y_2, \ldots\ldots\ldots, x_n, y_n)^T \qquad (3)$$

5. COMBINED STAGE

5.1. Modeling Gray-Level Appearance Knowledge

The main idea is to gather the gray level information in a region around each control point throughout the training set, concentrating on the gray profiles along a line passing through the control point in the direction of the selected origin (average center of mass).

For every control point *j* in the image i of the training set, a gray level profile g_{ij} is extracted, of length p pixels, centered at the control point. Instead of using the raw intensities along the profile, we utilize the normalized derivative in order to reduce the effect of global intensity changes. The gray level profile of the control point *j* in the image *i* is a vector of p values. With this we obtain a statistical model for the gray levels around each control point *j* (24 control points) represented by y_j and C_{yj} as shown in figure 1.

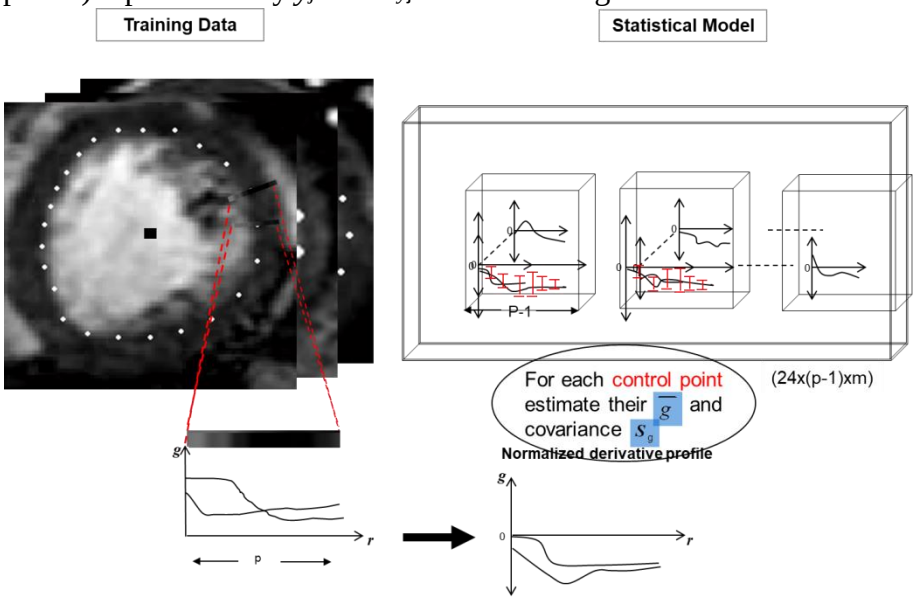

Figure 1 Building Knowledge based model

5.2. Searching Using Gray Appearance Knowledge

The modeling of gray level statistics around each control point can be used to determine the adjustment of each control point (x_j) so that a better model-to-data fit is obtained.

The search is applied along a line passing through the control point in the direction of the average center of mass. In this way, we obtain a sample profile. Within this sample profile we look for a sub-profile with characteristics that match the ones obtained from training. In order to do so, the gray level values are collected along the sample profile, compute the derivative and normalize. We then search within the normalized derivatives sample profile (having length *s*, $s > p$) for a sub-profile that matches the mean normalized derivative profile (of length *p*) obtained from the training set.

The sub-profile S_j along the control point j is given by

$$S_j = [S_{j1}\, S_{j2} \ldots\ldots S_{jp}]^T \quad (4)$$

The derivative sub-profile of control point j will be of length *p -1* as follows:

$$dS_j = [S_{j2} - S_{j1}\, S_{j3} - S_{j2} \ldots\ldots S_{jp} - S_{jp-1}]^T \quad (5)$$

The normalized derivative sub-profile becomes

$$y_{jp} = \frac{dS_j}{\sum_{k=1}^{p-1} |dS_{jk}|} \tag{6}$$

Now examine y_{jp} that match y_j (the mean normalized derivative profile obtained from the training set of images). Denoting the sub-interval y_{jp} centered at the d^{th} pixel of y_{jp} by $h(d)$, then find the value of d that makes the sub-interval $h(d)$ similar to y_j . This can be done by minimizing the following square error function with respect to d.

$$f(d) = (h(d) - \bar{y}_i)^T C_{yj}^{-1}(h(d)) - \bar{y}_j) \tag{7}$$

The advantage of using the defined square error function in equation 7, it measures the distance of the sample from the model mean y_j , in terms of the covariance C_{yj} , making it very sensitive to inter-variable changes in the training data. Also it is linearly related to the log of the probability that y_{jp} is drawn from the distribution. Minimizing $f(d)$ is equivalent to maximizing the probability that y_{jp} comes from the distribution.

6. RESULTS AND DISCUSSION

The method was tested on sequence of 220 MR images of deformable organ to locate the inner cavity of the left ventricle of heart from different cases. Images were acquired using a 1.5T whole body scanner (Intera CV, Philips Medical Systems) with Master Gradients (slew rate 150 T/m/s, amplitude 30 mT/m) and a 5-element phased-array cardiac coil. Three short survey scans were performed to define the position and true axis of the left ventricle. Afterwards, wall motion was imaged during breath holding in long and short-axis slices using a steady state free precession sequence, which provides an excellent demarcation of the endocardium. Cardiac synchronization was achieved by prospective gating. The cine images were recorded with 23 heart phases (23 frames per heart cycle). Each frame is 256x256 pixels with a slice thickness of 10mm. For each frame a region of interest was extracted of size 95x95 pixels. Figure 5 demonstrates using the appearance knowledge search, as the search progresses more suitable adjustments are made. The final convergence (the max control point iteration was 19 iterations) the method is compared with 2 approaches the first approach is GVF- snake which has advantages over other active contour models are its insensitivity to initialization, its ability to move into boundary concavities, and its large capture range. Which make the GVF snakes a good model for comparison. The second approach is AAMs is an extension of ASM using combined principle component analysis of the landmarks and pixel values within the object is made which allows the generation of images. The iterative steps in the optimization of the segmentation are steered by the difference between the true pixel values and the modeled pixel values within the object.

The results for the whole model were recorded and compared based on the square error distance (point to point) between the final best fitting given by proposed model and the hand-drawn contour. Figure 2 shows the mean errors with ±standard deviation for every control point. The final error is averaged for each training group. The mean error difference in pixels between the training groups is almost the same, which shows how the stability of the model even with the variation of training data set. The maximum distance mean error of 2.54 pixels from the ground truth contour, which also points to the satisfied accuracy, reached using the combined proposed method as.

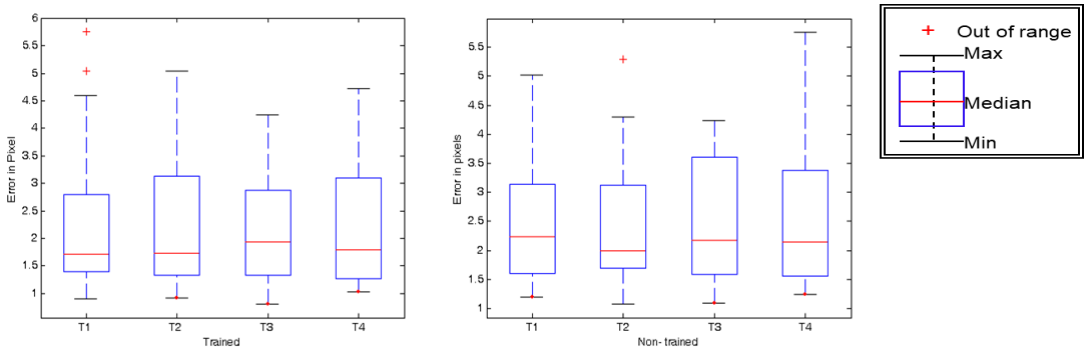

Figure 2 Left: The evaluation of the proposed model using the training set (T) against itself. Right: The evaluation of the proposed model using the training set (T) against non-trained set (S). Each case shows the range of error in pixels.

The proposed combined approach enriches in the large capture range than the GVF snakes this is because that the search technique does not fall in a local minimum problem. Due to the learning from the training set, since the model points are not always placed on the strongest edge in the locality; they may represent a weaker secondary edge. This increases the performance of the proposed model as shown in figure 3. On the other hand, the connectivity between the contour control points for deformation in the GVF model is better than the proposed approach, since the search technique is applied for every control point separately, without having any related curvature features between each other. Figure 4 shows mean error distance for each control point with their standard deviation. It is demonstrated that the performance of the search technique used by the proposed combined model is better, giving the average mean distance error of 2.41 pixels, while the average mean distance error by the GVF snakes model is 3.8 pixels.

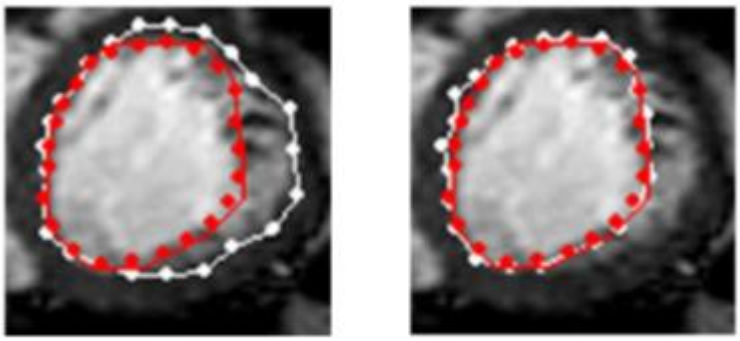

Figure 3 Left: The final contour (white) after applying the proposed model. Right: The final contour (white) after applying the GVF snake. Both are initialized with the estimated contour (red).

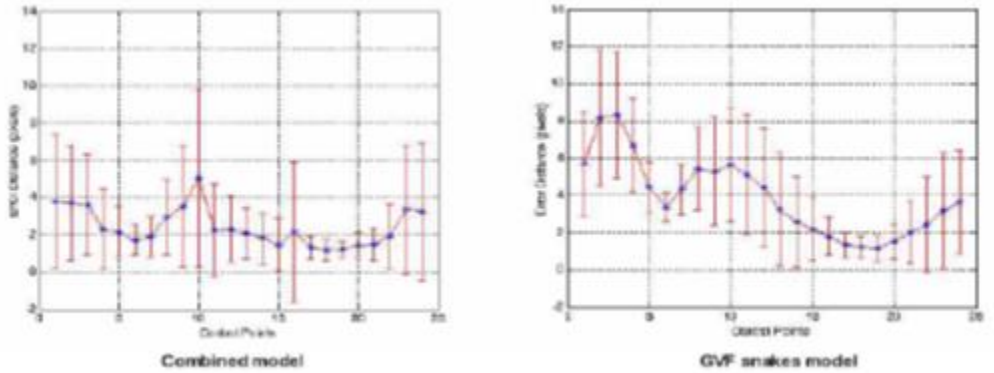

Figure 4 Distance mean error of combined model and GVF snakes.

The AAM has the ability to overpass the structures adjacent to the boundary, but still the fundamental drawbacks of the AAM makes our proposed model better. The drawbacks are summarized in the following points:

- AAMs are dependent on a good initialization.
- The matching phase is achieved by building a prior knowledge of how to adjust the model parameters during image matching. Several crucial questions remain unanswered such as: How many displacements should be used? How large should the displacements be? Should all parameters (i.e. rotation, translation and scale) be displaced at once or separately? Should the displacements be done in a deterministic or random fashion?
- The model can only deform in ways observed in the training set. If the contour exhibits a particular type of deformation not present in the training set, the model will not fit to it.

In conclusion, figure 5 compares the accuracy of the three models starting from the same position. We can see that the combined model achieved less distance error from the ground truth than the other two approaches.

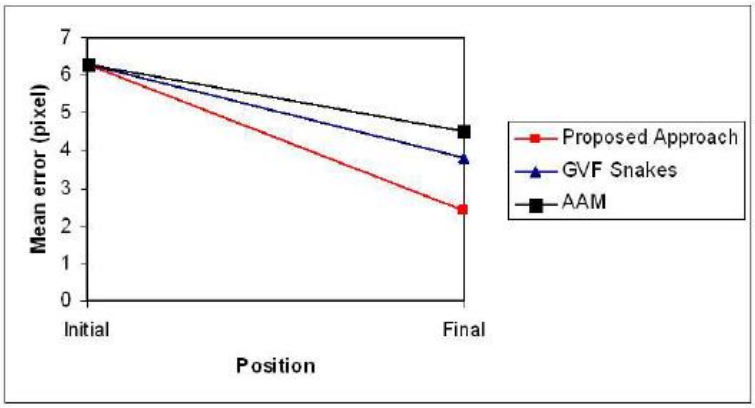

Figure 5 Comparing the GVF, AAM against proposed method.

7. CONCLUSIONS

The proposed model is evaluated and compared with two high level approaches. We showed how the data set is organized in the evaluation and training, and defining a measurement depending on comparison the model to ground truth. The results were evaluated and presented in three main stages: Demonstration of low-level model, evaluation of the combined low-high approach, and comparing the results with gradient vector flow snakes approach and active appearance approach. The results showed that our model gives high performance than other models in the following points:

- The developed model does not need to be good initialized. Since using morphological scale-space decomposition based on multi-scale spatial analysis, and defining the descriptor scale that gives constant values for structures of constant width, inherit the localization of edges. Where most of the applied method in the segmentation of deformable border, need first to assume roughly where the contour is in the ROI.
- The developed model minimizes human initialization and interaction. The model is well suited to tracking the deformable boundary through image sequences.

REFERENCES

[1] El-Messiry H., Kestler H.A., Grebe O., Neumann H., Morphological Scale-Space Decomposition for Segmenting the Ventricular Structure in Cardiac MR Images,

Springer, Wittenberg T., Hastreiter P., Hoppe U., Handels H., Horsch A., Meinzer HP. (eds) Bildverarbeitung für die Medizin 2003.

[2] Haythem El-Messiry, Hans A. Kestler, Olaf Grebe, Heiko Neumann., Segmenting the Endocardial Border of the Left Ventricle in Cardiac Magnetic Resonance Images". IEEE computers in cardiology 2003 volume 30, pages 625-628.

[3] Sarah Elsharkawy, Haythem Elmessiry, and Mohamed Roushdy, Multi-channel Combined Local Global optical flow approach using photometric invariants, International Journal of Intelligent Computing and Information Science, Cairo, Egypt, Vol.11, No. 1, January 2011, pp.143-152.

[4] J.A. Bangham, P.D. Ling, R. Harvey, Scale-space from nonlinear filters, *Pattern Analysis and Machine Intelligence IEEE Transactions on*, vol. 18, pp. 520-528, 1996, ISSN 0162-8828.

[5] Yongjian Yu, Jue Wang, Enclosure Transform for Interest Point Detection From Speckle Imagery, *Medical Imaging IEEE Transactions on*, vol. 36, pp. 769-780, 2017, ISSN 0278-0062.

[6] Joanna Isabelle Olszewska, Christophe De Vleeschouwer, Benoit Macq, Multi-feature vector flow for active contour tracking, Acoustics Speech and Signal Processing 2008. ICASSP 2008. IEEE International Conference on, pp. 721-724, 2008, ISSN 1520-6149.

[7] Yong-Hwan Lee, Yukong Lee, Dong-Seok Yang, Je-Ho Park, Youngseop Kim, Facial Feature Extraction Using Enhanced Active Shape Model, *Information Science and Applications (ICISA) 2013 International Conference on*, pp. 1-2, 2013.

[8] Regonda Nagaraju and M. Janga Reddy, Review of Medical Image Segmentation with Statistical Approach - State of the Art and Analysis. International Journal of Computer Engineering & Technology, 8(2), 2017, pp.36–55.

[9] S.Sankara Narayanan and M.Ramakrishnan, Software as a Service: MRI Cloud Automated Brain MRI Segmentation and Quantification Web Services, International Journal of Computer Engineering & Technology, 8(2), 2017, pp. 38–48.